

Effects of high-temperature AlN buffer on the microstructure of AlGaN/GaN HEMTs

© S. Çörekçi[¶], M.K. Öztürk*, Hongbo Yu⁺, M. Çakmak*, S. Özçelik*, E. Özbay*

Department of Physics, Kırklareli University,
39160 Kırklareli, Turkey

* Department of Physics, Gazi University,
06500 Ankara, Turkey

⁺ Nanotechnology Research Center, Bilkent University,
06800 Ankara, Turkey

• Nanotechnology Research Center, Department of Physics, Department of Electrical and Electronics Engineering,
Bilkent University,
06800 Ankara, Turkey

(Получена 4 сентября 2012 г. Принята к печати 10 сентября 2012 г.)

Effects on AlGaN/GaN high-electron-mobility transistor structure of a high-temperature AlN buffer on sapphire substrate have been studied by high-resolution x -ray diffraction and atomic force microscopy techniques. The buffer improves the microstructural quality of GaN epilayer and reduces approximately one order of magnitude the edge-type threading dislocation density. As expected, the buffer also leads an atomically flat surface with a low root-mean-square of 0.25 nm and a step termination density in the range of 10^8 cm^{-2} . Due to the high-temperature buffer layer, no change on the strain character of the GaN and AlGaN epitaxial layers has been observed. Both epilayers exhibit compressive strain in parallel to the growth direction and tensile strain in perpendicular to the growth direction. However, an high-temperature AlN buffer layer on sapphire substrate in the HEMT structure reduces the tensile stress in the AlGaN layer.

1. Introduction

The GaN-based high-electron-mobility transistors (HEMTs) are strong candidates for high-power and high-frequency applications owing to the excellent properties of group-III nitride semiconductor materials [1–4]. The GaN-based HEMT structures are commonly grown on sapphire substrates on account of the lack of large native substrate. However, the lattice constant and thermal coefficient discrepancy between GaN and sapphire brings about a high dislocation density in the GaN and overgrown epitaxial layers, which adversely affects the performance of devices. In order to reduce the dislocation density in the epilayers, several techniques such as the lateral epitaxy overgrowth and various buffer layers growth have been used [5–7]. In recent years, the growth of GaN and AlGaN films on an AlN buffer layer or multi-buffer layers have been attracting interest [7–10].

On the other hand, a semi-insulating (SI) thick-GaN main layer is a necessity for HEMTs because it decreases parallel conduction between the source and the drain, and ensures a sharp channel pinch off [11,12]. A SI-GaN is usually achieved by means of intentional doping or tuning the growth conditions [12–14]. Apart from these methods, Yu et al. [15] developed a SI-GaN layer for AlGaN/GaN HEMT applications by using an AlN buffer layer on sapphire substrate. Consequently, the AlN buffer layer has a critical important for the device performance, and thereby its effects on the heterostructures needs to be understood.

In case of heteroepitaxial growth, a strong influence of the buffer layer on the structural properties and the

character of the growth of subsequent layers has been well known [7,9,16,17]. We, too, had confirmed this in one of our previous studies [18]. In this study, we report the effects on the crystalline quality, dislocation density, and surface morphology of AlGaN/GaN-HEMTs of an HT-AlN (high-temperature AlN) buffer layer on c -plane sapphire substrate. We also evaluated the strain status of GaN and AlGaN epitaxial layers in the HEMT structures.

2. Experimental method

The unintentionally doped AlGaN/GaN-HEMTs used in the present study were grown on c -plane sapphire substrates in a low-pressure MOCVD reactor (Aixtron 200/4 HT-S) by using standard trimethylgallium (TMGa), trimethylaluminum (TMAI), and ammonia (NH_3) as Ga, Al, and N sources, respectively. Prior to the epilayer growth, the substrates were annealed at 1100°C for 10 min to remove the surface oxides. For sample with the buffer layer, the growth was initiated with the deposition of a 15-nm-thick low-temperature AlN nucleation layer (NL) at 840°C . Then, the reactor temperature was ramped to 1150°C and a 500-nm-thick HT-AlN buffer layer was grown. A sample without the buffer was deposited on a 25-nm-thick low-temperature GaN NL, for comparison a. The NL thickness and annealing process of this sample were carefully calibrated to obtain highly resistive character. Finally, for both samples, an undoped 2000-nm-thick GaN main layer, 25-nm-thick AlGaN barrier layer, and 3-nm-thick GaN top layer were grown at same growth temperature and reactor pressure. The HEMT structures with and without the HT-AlN buffer were labeled as samples A and B.

[¶] E-mail: scorekci@kirkklareli.edu.tr

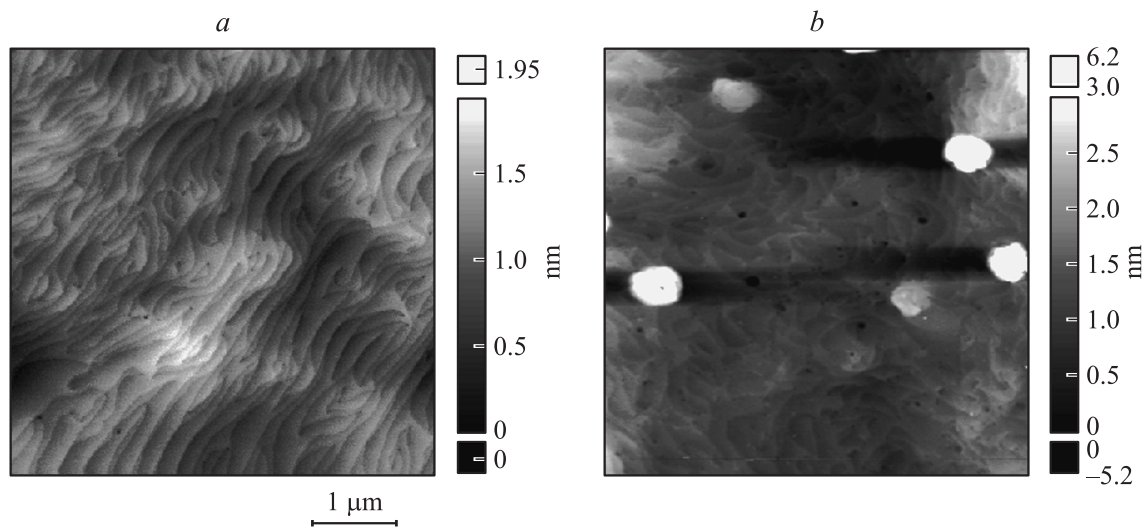


Figure 1. AFM scans with a $5 \times 5 \mu\text{m}^2$ area of the samples: (a) A and (b) B. Dark to white color variance corresponds to pit to hill variance on the surface of the samples.

The structural quality and strain state of the samples were examined by XRD measurements using a Bruker D8-Discover high-resolution diffractometer system. The surface morphology of the samples was characterized by AFM observations using an Omicron variable temperature (VT) STM/AFM instrument.

3. Results and discussion

In order to understand the surface properties of the samples, AFM scans were performed over a small area of $5 \times 5 \mu\text{m}^2$. Fig. 1 shows AFM images obtained from the GaN top surfaces of the HEMT structures. As seen from these images, sample A with the buffer has a well-defined step-terrace structure. However, sample B without the buffer displays pits and hillocks on the surface besides unclear step terraces. The pit and hillock densities of this sample were estimated as $5.6 \cdot 10^7$ and $2.4 \cdot 10^7 \text{ cm}^{-2}$ by the number of pits and hillocks from the image of $5 \times 5 \mu\text{m}^2$, respectively. The observed step-terrace formation on the surfaces of the samples reveals step-flow growth. On the other hand, the majority of the steps on the surfaces were terminated at dark spots in the images. It is rather well known that there are three kinds

of threading dislocations (TDs) in a GaN epilayer: pure screw (*c*-type), pure edge (*a*-type), and mixed (*c* + *a*)-type. The intersection of a TD except for the pure edge one with the free surface leads to a step termination on a single crystal surface and hence, the step termination density is related to the screw or mixed TD density [19]. The density of step terminations is in the range of 10^8 cm^{-2} on the surface of sample A. The step termination density was not distinguishable from sample B, on account of its rough surface. However, from the step-terrace structure and lateral sizes of the terraces, it is apparent that the step termination density of sample A is lower than that of sample B. Additionally, the root-mean-square (rms) values of samples A and B were obtained as 0.25 and 0.66 nm over a scan area of $5 \times 5 \mu\text{m}^2$, which are in agreement with the lateral sizes of the terraces on the surfaces. Consequently, AFM observations clearly indicated that sample A grown by using an HT-AlN buffer layer on sapphire substrate has a good-quality surface with an rms value of 0.25 nm and a regular step-terrace structure as opposed to the inferior surface of sample B grown by a low-temperature GaN NL only.

Fig. 2 shows Bragg reflections from the symmetric plane (0002) and asymmetric plane (10 $\bar{1}$ 2) of the GaN layers in the samples. Gaussian type (0002) reflections result from the mosaicity of the layers [20,21]. In this case, it is clear that GaN main layer without the buffer

Structural parameters of GaN and AlGaIn in samples A and B

Layer	Sample	FWHM ($^\circ$)		TD density (cm^{-2})		Strain	
		(0002)	(10 $\bar{1}$ 2)	D_{screw}	D_{edge}	ϵ_c	ϵ_a
GaN	A	0.078	0.104	$1.6 \cdot 10^8$	$7.4 \cdot 10^8$	-0.01007	0.01016
	B	0.116	0.342	$3.5 \cdot 10^8$	$8.1 \cdot 10^9$	-0.01672	0.00803
AlGaIn	A	—	—	—	—	-0.00437	0.00888
	B	—	—	—	—	-0.00771	0.02028

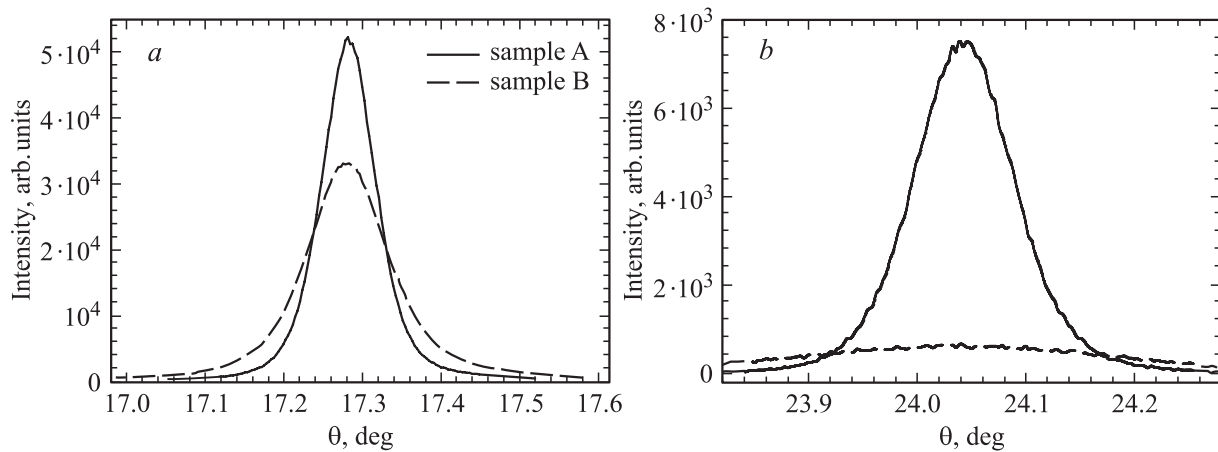


Figure 2. Bragg reflections of the samples: *a* — symmetric GaN (0002), *b* — asymmetric GaN (10 $\bar{1}2$).

in sample B has a more mosaic structure because of the wide spread of the reflection. As is already well known, the broadening of the X-ray reflections is related to the crystalline quality of epitaxial layers, which is denoted by the full-width at half-maximums (FWHMs) of the peaks. The FWHMs of samples A and B were determined as 0.078° for the GaN(0002) reflections and 0.104° , 0.342° for the GaN(10 $\bar{1}2$) reflections as listed in Table. As is clearly seen, the FWHM values of sample A are lower than those of sample B. These results show that the GaN in sample B has a poor quality, which seems in harmony with the inferior surface consists of pits and hillocks of the same sample. The X-ray reflections are broadened by limited crystallite size, out-of-plane and in-plane misorientations of crystallites (tilt and twist), and heterogeneous strain (microstrain) in epitaxial films [22,23]. In addition, the tilt and twist misorientations are associated with the screw (*c*-type) and edge (*a*-type) TDs in the films [23]. Unfortunately, dislocations lead to drain-current collapse in AlGaIn/GaN HEMTs [24]. The dislocation density of GaN in the samples was estimated from the following equations [25],

$$D_{\text{screw}} = \frac{\beta_{(0002)}^2}{4.35b_{\text{screw}}^2}, \quad D_{\text{edge}} = \frac{\beta_{(10\bar{1}2)}^2}{4.35b_{\text{edge}}^2} \quad (1)$$

where D_{screw} is the screw-type TD density, D_{edge} is the edge-type TD density, β is the FWHM of X-ray reflections, and b is the Burgers vector length of the dislocation ($b_{\text{screw}} = 5.1855 \text{ \AA}$, $b_{\text{edge}} = 3.1890 \text{ \AA}$). The screw and edge TD densities in GaN were estimated as $1.6 \cdot 10^8$, $7.4 \cdot 10^8 \text{ cm}^{-2}$ for sample A and $3.5 \cdot 10^8$, $8.1 \cdot 10^9 \text{ cm}^{-2}$ for sample B, respectively. From these results, it is clearly seen that the TD density of the GaN main layer in sample A decreases due to the presence of an HT-AlN buffer layer on sapphire substrate, which is consistent with our previous study [18] on structural, morphological, and optical properties of AlGaIn/GaN heterostructures with AlN buffer and interlayer. In addition, the estimated screw

dislocation densities of the samples show conformity with the step termination densities in the AFM images.

On the other hand, the density of the edge threading dislocations (TDs) for both samples is higher than that of the screw ones, which is typical for epitaxial GaN layers. This result is due to the smaller nucleation energy of the edge TDs [26]. Furthermore, the edge dislocation density of sample B is approximately higher one order of magnitude than that of sample A, which can be related to the nucleation and annealing process of sample B. Look et al. [27] found that the edge-type TDs in GaN are electrically active. Hence, the reduction of edge TD densities in the samples is important for achieving the high HEMT performance. Fini et al. [28] reported that the low angle grain boundaries are the main source of the edge-type TDs in the GaN films. Qian et al. [29] show that the grains are formed during the coalescence of the islands in NL at the initial stage of GaN growth due to island misorientation. Xu et al. [30] found that a higher island density leads more grain boundary. Also, they indicated that the size and density of islands strongly influence the diffusion of oxygen impurities from sapphire substrate into GaN. In this context, the high TD density of sample B, in which a major contributor is the edge TDs, means the high island density and small island size in NL, and to be limited of the oxygen diffusion.

The structural quality of GaN main layer and AlGaIn barrier layer in the samples were characterized in detail utilizing reciprocal space maps (RSMs). Fig. 3 shows the two RSMs having an elliptical shape recorded around the asymmetric (10 $\bar{1}5$) Bragg reflections for samples A and B. The elliptic nature of the RSMs is typical for III-nitrides and associated with mosaicity of epitaxial layers [31].

An epitaxial layer with high dislocation density are often described by the mosaic model [32], in which the layer is assumed to consist of single crystalline blocks with lateral and vertical coherence lengths. The rotation (tilt and twist) and sizes of the mosaic blocks are related to the intensity distributions in RSMs [32]. Thus, the larger broadening appeared along the Q_x and Q_z axes for GaN in sample B

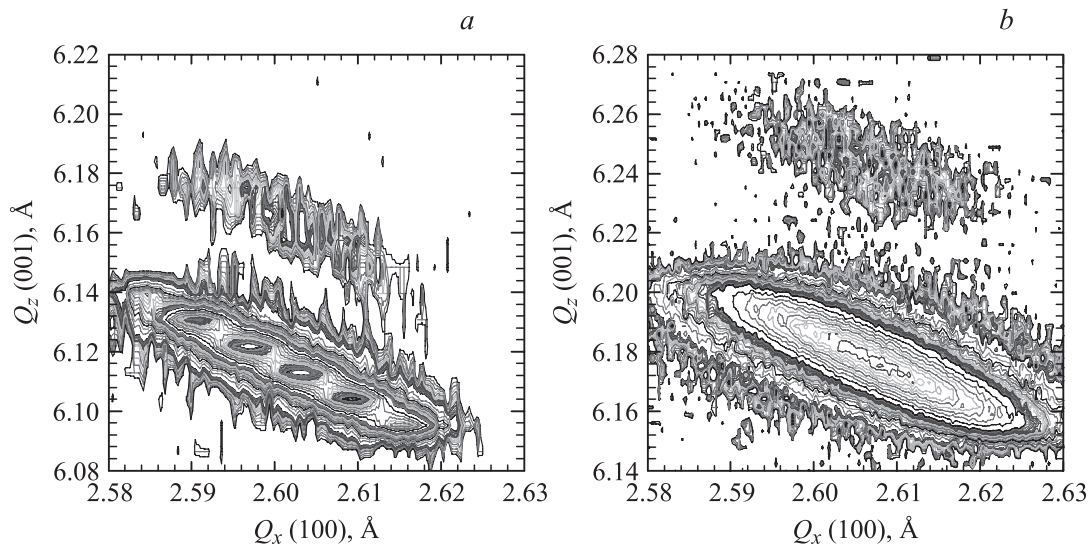


Figure 3. RSMs recorded around the asymmetric $(10\bar{1}5)$ reflections for samples (a) A and (b) B.

is due to the limited coherence lengths and relatively high tilt- and twist-angles of the layer. According to the report of Chierchia et al. [32], the inclination of the main axis of the ellipses with respect to the Q_x axis increases with the grain diameter. In this context, the larger inclination of GaN in sample A implies the larger grain diameter, which is in good agreement with the relatively wide terraces in AFM image of the same sample.

On the other hand, the intensity maximum of AlGaN peak in both samples is aligned parallel to that of GaN peak, which implies a pseudomorphic growth for the AlGaN layers. In order to clarify this, the in-plane (*a*) and out-of-plane (*c*) lattice constants of the GaN and AlGaN were extracted and strain status of the layers was evaluated by utilizing the lattice constants. The *a*-lattice constant of the AlGaN and GaN for both samples was very similar to each other. Kisielowski et al. demonstrated presence of a biaxial strain in GaN thin films on account of the growth on lattice-mismatched substrates and post-growth cooling, and a hydrostatic strain due to the point defects [33]. The ϵ_c and ϵ_a strain amounts in the GaN and AlGaN along the *c*- and *a*-axes were calculated and the results were listed in Table. The *a* and *c* lattice constants were taken to be 3.1890 and 5.1855 Å for unstrained GaN, respectively. As can be seen in Table, the GaN and AlGaN layers in the samples are compressively strained in parallel to the growth direction (in the *c*-direction), while they are tensile strained in perpendicular to the growth direction (in basal plane). These results are in agreement with a previous report [34] showing that the layers grown on *c*-plane sapphire by a nucleation layer are tensile strained. Strain character of heteroepitaxially grown GaN layers on sapphire substrates is determined by the superposition of tensile/compressive stress result from point defects in the layers and growth on the lattice-mismatched substrates [33,35], biaxial tensile stress associated with the coalescence process of the

islands [34,36,37], and compressive stress caused by cooling of the layers to room temperature [34]. In this case, the tensile strain in *a*-axis of the GaN is probably originated from the density of point defects and/or the coalescence process. On the one hand, the high edge TD density of sample B shows that the strain in GaN partially release. The relatively low ϵ_a -strain of GaN in sample B can be related to the layer thickness, non-stoichiometric growth, oxygen concentration, or coalescence process on different surfaces of the GaN islands. On the contrary, the tensile strain in *a*-axis of AlGaN barrier layer in sample B is higher than that of sample A. This results shows that an HT-AlN buffer layer on sapphire substrate reduces the tensile stress in the barrier layer of the HEMT structure. Finally, the high quality of sample A with HT-AlN buffer, which was revealed in the AFM observations, was confirmed by an improvement in the microstructural quality from the HRXRD measurements.

4. Conclusion

We investigated the effects of an HT-AlN buffer layer on microstructure AlGaN/GaN-HEMTs grown on sapphire substrates by low-pressure MOCVD. The buffer layer remarkably improves to the structural quality of the epitaxial layers in the HEMT structure and decreases the propagating of the threading dislocations into GaN main layer. We also evaluated the strain status of GaN main layer and AlGaN barrier layer. The experimental results reveal that these layers are compressively strained in the *c*-axis and tensile strained in the *a*-axis. However, an HT-AlN buffer layer on *c*-plane sapphire substrate reduces the tensile stress in the AlGaN barrier.

ACKNOWLEDGMENTS: This work was supported by the Turkish State Planning Organization, DPT and the Scientific and Technological Research Council of Turkey,

TUBITAK. We would like to thank an anonymous referee for his instructive comments for improving the clarity and quality of this paper.

References

- [1] U.K. Mishra, Y.-F. Wu, B.P. Keller, S. Keller, S.P. Denbaars. IEEE Trans. Microwave Theory and Tehcniques, **46**, 756 (1998).
- [2] Y.-F. Wu, D. Kapolnek, J.P. Ibbetson, P. Parikh, B.P. Keller, U.K. Mishra. IEEE Trans. Electron. Dev., **48**, 586 (2001).
- [3] L. Shen, S. Heikman, B. Moran, R. Coffie, N.-Q. Zhang, D. Buttari, I.P. Smorchkova, S. Keller, S.P. DenBaars, U.K. Mishra. IEEE Electron. Dev. Lett., **22**, 457 (2001).
- [4] M. Umeno, T. Egawa, H. Ishikawa. Mater. Sci. Semcond. Proc., **4**, 459 (2001).
- [5] H. Jiang, T. Egawa, M. Hao, Y. Liu. Appl. Phys. Lett., **87**, 241 911 (2005).
- [6] X.L. Fang, Y.Q. Wang, H. Meidia, S. Mahajan. Appl. Phys. Lett., **84**, 484 (2004).
- [7] C.W. Kuo, Y.K. Fu, C.H. Kuo, L.C. Chang, C.J. Tun, C.J. Pan, G.C. Chi. J. Cryst. Growth, **311**, 249 (2009).
- [8] J.-S. Ha, H.-J. Lee, S.W. Lee, H.J. Lee, S.H. Lee, H. Goto, M.W. Cho, T. Yao, S.-K. Hong, R. Toba, J.W. Lee, J.Y. Lee. Appl. Phys. Lett., **92**, 091 906 (2008).
- [9] Q.M. Fu, T. Peng, F. Mei, Y. Pan, L. Liao, C. Liu. J. Phys. D: Appl. Phys., **42**, 035 311 (2009).
- [10] S. Çörekçi, M.K. Öztürk, A. Bengi, M. Çakmak, S. Özçelik, E. Özbay. J. Mater. Sci., **46**, 1606 (2011).
- [11] Z. Chen, Y. Pei, S. Newman, R. Chu, D. Brown, R. Chung, S. Keller, S.P. DenBaars, S. Nakamura, U.K. Mishra. Appl. Phys. Lett., **94**, 112 108 (2009).
- [12] S.M. Hubbard, G. Zhao, D. Pavlidis, W. Sutton, E. Cho. J. Cryst. Growth, **284**, 297 (2005).
- [13] S. Heikman, S. Keller, S.P. DenBaars, U.K. Mishra. Appl. Phys. Lett., **81**, 439 (2002).
- [14] Z. Bougrioua, I. Moerman, L. Nistor, B. Van Daele, E. Monroy, T. Palacios, F. Calle, M. Leroux. Phys. Status Solidi A, **195**, 93 (2003).
- [15] H. Yu, D. Çalışkan, E. Özbay. J. Appl. Phys., **100**, 033 501 (2006).
- [16] M. Miyoshi, H. Ishikawa, T. Egawa, K. Asai, M. Mouri, T. Shibata, M. Tanaka, O. Oda. Appl. Phys. Lett., **85**, 1710 (2004).
- [17] B. Poti, M.A. Tagliente, A. Passaseo. J. Non-Cryst. Sol., **352**, 2332 (2006).
- [18] S. Çörekçi, M.K. Öztürk, B. Akaoğlu, M. Çakmak, S. Özçelik, E. Özbay. J. Appl. Phys., **101**, 123 502 (2007).
- [19] D. Kapolnek, X.H. Wu, B. Heying, S. Keller, B.P. Keller, U.K. Mishra, S.P. DenBaars, J.S. Speck. Appl. Phys. Lett., **67**, 1541 (1995).
- [20] V.V. Mamutin, V.A. Vekshin, V.Yu. Davydov, V.V. Ratnikov, A.Yu. Kudriavtsev, B. Ya. Ber, V.V. Emtsev, S.V. Ivanov. Phys. Status Solidi A, **176**, 373 (1999).
- [21] V. Tasco, A. Campa, I. Tarantini, A. Passaseo, F. González-Possada, A. Redondo-Cubero, K. Lorenz, N. Franco, E. Muñoz. J. Appl. Phys., **105**, 063 510 (2009).
- [22] M.E. Vickers, M.J. Kappers, R. Datta, C. McAleese, T.M. Smeeton, F.D.G. Rayment, C.J. Humphreys. J. Phys. D: Appl. Phys., **38**, A99-A104 (2005).
- [23] H. Jiang, T. Egawa, M. Hao, Y. Liu. Appl. Phys. Lett., **87**, 241 911 (2005).
- [24] S. Arulkumar, T. Egawa, H. Ishikawa, T. Jimbo. Appl. Phys. Lett., **81**, 3073 (2002).
- [25] C.G. Dunn, E.F. Koch. Acta Metall. **5**, 548 (1957).
- [26] L. Sugiura. J. Appl. Phys., **81**, 1633 (1997).
- [27] D.C. Look, J.R. Sizelove. Phys. Rev. Lett., **82**, 1237 (1999).
- [28] P. Fini, X. Wu, E.J. Tarsa, Y. Golan, V. Srikant, S. Keller, S.P. Denbaars, J.S. Speck. Jpn. J. Appl. Phys., **37**, 4460 (1998).
- [29] W. Qian, M. Skowronski, M. De Graef, K. Doverspike, L.B. Rowland, D. Gaskill. Appl. Phys. Lett., **66**, 1252 (1995).
- [30] F.J. Xu, J. Xu, B. Shen, Z.L. Miao, S. Huang, L. Lu, Z.J. Yang, Z.X. Qin, G.Y. Zhang. Thin Sol. Films, **517**, 588 (2008).
- [31] V. Darakchieva, B. Monemar, A. Usui. Appl. Phys. Lett., **91**, 031 911 (2007).
- [32] R. Chierchia, T. Böttcher, H. Heinke, S. Einfeldt, S. Figge, D. Hommel. J. Appl. Phys., **93**, 8919 (2003).
- [33] C. Kisielowski, J. Krüger, S. Ruvimov, T. Suski, J.W. Ager III, E. Jones, Z. Liliental-Weber, M. Rubin, E.R. Weber, M.D. Bremser, R.F. Davis. Phys. Rev. B, **54**, 17 745 (1996).
- [34] S. Hearne, E. Chson, J. Han, J.A. Floro, J. Fiegel, J. Hunter, H. Amano, I.S.T. Tsong. Appl. Phys. Lett., **74**, 356 (1999).
- [35] V.S. Harutyunyan, A.P. Aivazyan, E.R. Weber, Y. Kim, Y. Park, S.G. Subramanya. J. Phys. D: Appl. Phys., **34**, A35-A39 (2001).
- [36] W.D. Nix, B.M. Clemens. J. Mater. Res., **14**, 3467 (1999).
- [37] R. Chierchia. *Strain and crystalline defects in epitaxial GaN layers studied by high-resolution X-ray diffraction* (Bremen. 2007).

Редактор Т.А. Полянская